J Mater Sci (2007) 42:4562–4574
DOI 10.1007/s10853-006-0550-5

A constitutive equation for the dynamic deformation behavior of polymers

F. J. Zerilli · R. W. Armstrong

Received: 4 February 2006 / Accepted: 8 June 2006 / Published online: 16 February 2007

Abstract A constitutive equation based on the generalized concept of thermally activated flow units is developed to describe the stress–strain behavior of polymers as a function of temperature, strain-rate, and superposed hydrostatic pressure under conditions in which creep and long-term relaxation effects are negligible. The equation is shown to describe the principal features of the dynamic stress–strain behavior of polytetrafluoroethylene and, also, the yield stress of polymethylmethacrylate as a function of temperature and strain rate. A key feature of the model, not utilized in previous constitutive equation descriptions, is an inverse shear stress dependence of the shear activation volume. In contrast to metal deformation behavior, an enhanced strain hardening with increasing strain at higher strain rates and pressures is accounted for by an additional rate for immobilization of flow units. The influence of hydrostatic pressure enters through a pressure activation volume and also through the flow unit immobilization term. The thermal activation model is combined with a temperature dependent Maxwell–Weichert linear viscoelastic model that describes the initial small strain part of the stress strain curve.

F. J. Zerilli
Research and Technology Department, Naval Surface Warfare Center, Indian Head, MD 20640-5035, USA

R. W. Armstrong (✉)
Center for Energetic Concepts Development, University of Maryland, College Park, MD 20742-5035, USA
e-mail: rona@eng.umd.edu

Introduction

Thermal activation

Following pioneering work by Eyring [1, 2], an Arrhenius form of thermally activated constitutive equation for the temperature and strain rate dependence of flow stress has been well established for a wide variety of solid materials over appropriate temperature and strain rate regimes. For metals, the modeled constitutive equation parameters for different situations have been quantitatively matched with a variety of dislocation mechanisms. Implicit in the general thermal activation model description, however, is the consideration only that permanent deformation occurs inhomogeneously under an applied shear stress through the movement of individual flow units, that is, structures in a material responsible for initiating shear flows, by surmounting local obstacles (potential barriers) to displacement.

In Fig. 1 is displayed a so-called master curve reported by Bauwens-Crowet [3], and importantly discussed [4, 5], for the compressive yield stress dependence on strain rate of polymethylmethacrylate (PMMA) as derived from tests conducted over a range of temperatures and strain rates. Of particular importance in Fig. 1 is the dependence of the flow stress σ on strain rate $\dot{\varepsilon}$, at constant temperature T, which determines the activation volume, V, for the thermally activated flow process through the relation

$$\left(\frac{\partial \sigma}{\partial \ln \dot{\varepsilon}}\right)_T = \frac{kT}{V} \tag{1}$$

where k is Boltzmann's constant. In Fig. 1, a curve drawn based on the assumption that V is inversely

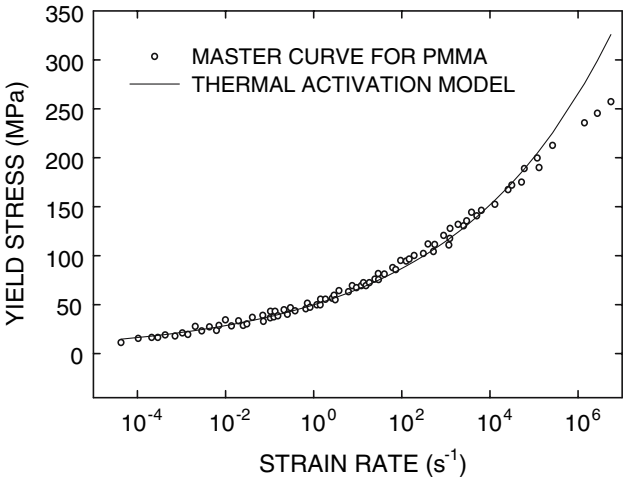

Fig. 1 Thermal activation model with activation volume proportional to inverse of thermal stress compared to master curve points for PMMA reported by Bauwens-Crowet [3]

proportional to the thermal component of stress shows good agreement with the set of master points except at the highest strain rates. The demonstrated agreement can be considerably improved as we will see later.

For metals, the shear activation volume is specified as the product of an activation area and, within the areal plane, a dislocation Burgers vector that quantifies the characteristic flow unit displacement. Armstrong [6] showed that the activation volume followed an inverse dependence on the thermal component of stress for a wide variety of metal crystals and polycrystals whose deformation properties were proposed to be controlled by quite different dislocation mechanisms. Also, the inverse dependence on thermal stress was pointed out to be a good approximation to quantitative theoretical model results for two quite different thermally activated dislocation mechanisms [7]. Thus, the reciprocal activation volume dependence on thermal component of stress in the metal case was shown to have a more general applicability than being restricted to a particular dislocation mechanism; and, Fig. 1 for a supposedly structure less polymer, gives indication of applicability of the dependence to a wider class of materials. To some extent, the present consideration is separate from the pioneering researches that have been done, only with partial success, thus far, to identify the polymer flow unit analogs of crystal dislocations [8–10], say, as compared to the properties of long chained molecules [11, 12].

Complexities of solid polymeric materials

The agreement between the model calculation and the summary of experimental results in Fig. 1 is achieved without requirement of the next step complication of more fully characterizing the flow unit characteristics for the viscoelastic/plastic behavior of polymeric materials. Other researchers have pursued the physical characterizations of such activation volume measurements [13] while the message here, in any case, is that Eyring's thermal activation model is applicable to polymers in the presently described manner, in agreement with other results reported earlier in several investigations [14, 15]. Part of the complication of accounting for the deformation behavior stems from the great range of internal structures that may be achieved in bulk polymeric materials. Polymers may exist in perfect crystal form, in an amorphous or glassy state, or some mixture of amorphous and crystalline material. The constitutive relation is affected by many factors including the degree of crystallinity, microcrystal sizes, characteristics of the amorphous material encasing crystal subunits, molecular chain characteristics, molecular weight distribution, internal porosity, and presence of water or plasticizer. The yield and flow stress of polymers is strongly pressure dependent as well as temperature and strain rate dependent. Unlike metals, which exhibit low temperature plastic flow only in shear, polymers may have a significant unrecoverable strain component in hydrostatic compression. Compared to metals, polymers undergo relatively large elastic strains with strong strain rate, temperature, and pressure dependence of the elastic modulus. And often there exists limited experimental data due to a host of mechanical testing difficulties.

Other factors which ultimately must be addressed are the frequent occurrence of a ductile–brittle transition in polymers which becomes important at high strain rates, the brittleness which is associated with pressure effects, and the fracturing behavior associated with cracks, pores and inclusions.

Proposed model addresses strain rate, temperature, and pressure dependence

To reduce the complexity of the problem, we develop an equation which addresses only the temperature, strain-rate, and pressure dependence of the stress–strain relation. The small plastic component of strain in hydrostatic compression is not addressed, nor are such factors as brittleness and fracturing associated with strain-rate, temperature, and pressure effects. It is assumed that the strain-rates and temperatures are in the range in which creep and long-term relaxation effects are negligible. The model is three dimensional but isotropic. The extension to three dimensional non-isotropic conditions is left for future work.

The total strain is divided into a viscoplastic part and a viscoelastic part, the viscoplastic part being

described by a non-linear thermal activation dashpot analogous to that described by Eyring [2], and the viscoelastic part being described in terms of a Maxwell–Weichert linear viscoelasticity [16]. As will be seen, the Maxwell–Weichert model description of springs and dashpots is shown to produce reasonable agreement with storage shear modulus, logarithmic decrement, and relaxation moduli measurements. The aim, eventually, of such modeling effort is to connect with actual frequency-dependent relaxation processes in the material [17].

Combined elasticity, viscoelasticity, and viscoplasticity

A number of ways have been proposed to treat combined elasticity, viscoelasticity, and viscoplasticity. Linear or non-linear viscoelastic models without a definitive yield surface in which elastic and plastic strain coexist always have been described by a number of workers, including Johnston and Gilman [18] and Krausz and Eyring [19]. Viscoelastic models with a plastic flow surface were discussed by Perzyna [20]. A nice summary with references to relevant literature may be found in the article of Bardenhagen et al. [21]. We choose here to combine linear viscoelasticity to describe the initial small strain behavior with a viscoplastic model without a definite yield surface for the large strain behavior. Experimental evidence indicates that most, if not all, of the so-called plastic deformation is recoverable, given enough time or high enough temperature. This recovery is not treated in this work.

Applications to polytetrafluoroethylene and polymethylmethacrylate

The equations are shown to describe the major features of the reported stress–strain curves of semi-crystalline polytetrafluoroethylene (PTFE) as functions of temperature, pressure, and strain rate. The PTFE is assumed to have a density of 2.15 g cm^{-3} which would fix the degree of crystallinity in the range of 55–60%, depending on the concentration of microvoids.

PTFE is a good candidate for constructing a constitutive relation because it does not exhibit the necking instability in tension unlike many other polymers. Thus reported nominal load versus elongation tensile data may be accurately transformed to true stress–true strain data required for model development. However, it is a fairly complex material with a number of amorphous and polymorphic transitions. It also exhibits significant non-linear viscoelastic behavior [22] down to small strains of the order of 1%.

The yield stress of glassy PMMA can also be described quite well as a function of temperature and strain rate, provided the dependence of the yield stress upon the elastic shear modulus is taken into account. In addition, the resulting model allows some quantitative statements to be made concerning the ductile–brittle transition in PMMA.

Modeling pressure dependence

A number of empirical methods have been used to model the pressure dependence of the yield stress [23, 24] as well as more fundamental methods based on thermally activated flow [25, 26].

Among the empirical methods are included, for example, models with pressure dependent yield surfaces defined either by the Mohr–Coulomb yield condition

$$\tau - mp \leqslant \tau_0 \tag{2}$$

where τ is the shear stress, p is the pressure, m and τ_0 are constants, or by a yield criterion in which the first or second power of the Mises effective stress is expanded in a power series in the pressure [27, 28]

$$(J_2')^n = a_0 + a_1 J_1 + a_2 J_1^2 + \cdots \tag{3}$$

where J_1 (= –3 times the pressure) is the trace of the stress tensor and $J_{2'}$ (proportional to the square of the Mises stress) is the second invariant of the trace free part of the stress tensor, and n, typically, is 1 or 1/2. Such criteria are difficult to apply in modeling the stress–strain relation for polymers because the characteristic shape of the curves changes with pressure.

In this work, the viscoplastic flow stress is described by a pressure, temperature, strain-rate, and strain dependent relation between effective stress and effective strain

$$\sigma \equiv \sqrt{3 J_2'} = f(\varepsilon, \dot{\varepsilon}, T, p) \tag{4}$$

where the form of the pressure dependence is inferred from thermal activation considerations.

Polymer constitutive equation: viscoplastic component

Eyring's thermal activation theory

The basis of the thermal activation model is the theory of Eyring [1, 2] describing the rate of any process in

which matter rearranges by surmounting a potential energy barrier. When the potential barrier is sufficiently high, the rate in the forward direction exceeds the reverse reaction rate significantly and the plastic strain rate is given by the expression [29]

$$\dot{\varepsilon} = \dot{\varepsilon}_0 e^{-G/kT} \tag{5}$$

where G is the activation energy for the reaction, k is Boltzmann's constant, and T is the absolute temperature. G may be identified with the Gibbs free energy, so we may write

$$dG = -SdT - V_{ij}d\sigma_{ij} \tag{6}$$

so that at constant temperature

$$G = G_0 - \int V_{ij}d\sigma_{ij} \tag{7}$$

where σ_{ij} is the Cauchy stress tensor and the so called volumes of activation V_{ij} are functions of σ_{ij} and T. The repeated indices signify summation over the range of the indices. Stress is considered positive in tension.

For isotropic materials, there are only three independent components of stress so

$$V_{ij}d\sigma_{ij} = V_\sigma d\sigma + V_3 dJ_3' - V_p dp \tag{8}$$

where the effective stress $\sigma \equiv \sqrt{3J_{2'}}$, the pressure $p = -\frac{1}{3}\sigma_{kk}$, and J_2' and J_3' are the second and third invariants, respectively, of the trace free stress tensor. With the assumption that V_3 is zero,

$$G = G_0 - \int V_\sigma d\sigma + \int V_{kk}dp. \tag{9}$$

Further, we assume that V_σ is a function of effective stress and pressure and V_{kk} is a function only of pressure. Equation 5 may now be written

$$\int V_\sigma d\sigma = \int V_{kk}dp + G_0 + kT\ln(\dot{\varepsilon}/\dot{\varepsilon}_0). \tag{10}$$

Note that the effective stress activation volume previously defined by Eq. 1 follows directly from Eq. 10. Assuming that the effective stress activation volume depends inversely on the effective stress, choosing

$$V_\sigma = \frac{W_0(p)}{\sigma} \tag{11}$$

where W_0 is some function of pressure, and solving for the effective stress, Eq. 10 becomes

$$\sigma = B(p)e^{-\beta(p,\dot{\varepsilon})T} \tag{12}$$

where

$$B(p) = \sigma_0 \exp\left\{\frac{G_0 + \int V_{kk}dp}{W_0(p)}\right\} \tag{13}$$

and

$$\beta(p,\dot{\varepsilon}) = \frac{k}{W_0(p)}\ln(\dot{\varepsilon}_0/\dot{\varepsilon}). \tag{14}$$

Viscoplastic stress–strain behavior of polymers

In order to describe the viscoplastic stress–strain behavior of polymers, two thermally activated processes are considered, one associated with the initial yield behavior, the other associated with the subsequent strain hardening behavior. Thus the total flow stress is written

$$\sigma = B(p)e^{-\beta(p,\dot{\varepsilon})T} + \hat{\sigma}(\varepsilon,p)e^{-\alpha(p,\dot{\varepsilon})T} \tag{15}$$

where two terms of the form of Eq. 12 have been included. The presence of two separate deformation mechanisms was suggested in a differential scanning calorimetry study of glassy polymers by Hasan and Boyce [30]. Two distinct exotherms were found, one, at temperatures below the glass transition temperature, associated with the initial yield and strain softening behavior, the other, at temperatures above the glass transition temperature, associated with the strain hardening behavior.

The fit of master curve data for the yielding of PMMA shown in Fig. 1 was obtained from the first term in Eq. 15.

Strain hardening in polymers

Relative to the earlier discussion given in the Introduction, a number of shear-connected processes may play a role in the deformation of any given polymer: chain slippage, kinking and un-kinking of chains and related chain segment rotation, chain entanglement, chain scission, and cross-linking [8–12]. One or more of these processes will be important for a given polymer in a certain regime of temperature, strain-rate, and pressure. Whatever the processes, we adopt an extremely simplified picture and describe the aggregate result abstractly in terms of *units of flow* as defined by Kauzmann [31]. In Kauzmann's definition, units of flow are the ''structures in a body whose motions past one another make up the unit shear stress process... the unit of flow may be a single molecule or a group of many molecules, and the barrier may arise directly from the

repulsions between a few molecules or from some more complicated mechanism.'' The key consideration, however, in the present case, that allows us to go further is the inverse dependence of the flow unit ''volume'' on the thermal component of stress.

Here we consider an areal density of units of flow, ρ, which are presumably somewhat analogous to dislocations in crystalline materials—line defects which form the boundaries between slipped and unslipped regions of material. Gilman [32] was a pioneer in applying dislocation theory to amorphous materials and the need to replace the constant Burgers displacement in crystalline materials with the average of a fluctuating Burgers displacement in the amorphous material.

Extending such analogy further, we will assume that, at low temperatures, in the absence of thermal fluctuations, the flow stress is proportional to the square root of ρ

$$\hat{\sigma} = \hat{\alpha}\sqrt{\rho} \tag{16}$$

where $\hat{\alpha}$ is a constant. In crystalline materials, Eq. 16 results from the assumption that the force between flow units (dislocations or otherwise) is inversely proportional to the distance between them which, in turn, is a consequence of the elastic stress field resulting from the distortion produced by the flow unit.

Following Bergstrom's analysis for dislocations in iron [33], divide the flow unit density into a mobile flow unit density ρ_m and an immobile flow unit density ρ_i and assume that the mobile flow unit density is constant. Then the total flow unit density may be related to the plastic strain by the differential equation

$$\frac{d\rho}{d\varepsilon} = \frac{1}{b\lambda} - \omega\rho \tag{17}$$

where b is the average displacement produced by a flow unit, λ is the mean free path for immobilization of flow units, and ω is the rate for mobilization of flow units. We allow ω to be negative, this term then also contributing to the immobilization of flow units. If b, λ, and ω are constant, the equation is easily solved and the cold flow stress becomes

$$\hat{\sigma} = B_0\sqrt{(1 - e^{-\omega\varepsilon})/\omega}. \tag{18}$$

Note that $\varepsilon_c = \frac{1}{|\omega|}$ is a characteristic strain at which significant deviation from a parabolic stress/strain relation occurs. At temperatures above zero, this cold flow stress is reduced by the thermal activation factor $e^{-\alpha(p,\dot{\varepsilon})T}$.

Total viscoplastic component of deformation

The resulting viscoplastic component of the deformation is described by the equation

$$\sigma = Be^{-\beta T} + B_0\sqrt{(1 - e^{-\omega\varepsilon})/\omega}e^{-\alpha T} \tag{19}$$

where

$$\begin{aligned} \beta &= \beta_0 - \beta_1 \ln\dot{\varepsilon} \\ \alpha &= \alpha_0 - \alpha_1 \ln\dot{\varepsilon} \end{aligned} \tag{20}$$

and, neglecting their potential pressure dependence, β_0, β_1, α_0, α_1 are constants. From the experimental data for PTFE, ω depends approximately linearly on the pressure and logarithmically on the strain rate, so we choose

$$\omega = \omega_a + \omega_b \ln\dot{\varepsilon} + \omega_p p \tag{21}$$

where ω_a, ω_b, ω_p are constants. The form of the pressure dependence for the coefficients B and B_0 follows the result of Argon [34] who derived the expression

$$\tau = (a + cp)^{6/5} \tag{22}$$

for the low temperature shear yield stress of glassy polymers as a function of pressure. Argon's model is based on the thermally activated production of pair of kinks in the collection of interpenetrating smooth chain molecules comprising the polymer. Thus, we choose

$$\begin{aligned} B &= B_{pa}(1 + B_{pb}p)^{B_{pn}} \\ B_0 &= B_{0pa}(1 + B_{0pb}p)^{B_{0pn}} \end{aligned} \tag{23}$$

where the quantities B_{pa}, B_{pb}, B_{pn}, B_{0pa}, B_{0pb}, B_{0pn} are constants.

Polymer constitutive equation: viscoelastic component

A Maxwell–Weichert model is used to describe the initial viscoelastic stress. This model is placed in series with the non-linear dashpot described by Eq. 19 above as illustrated in Fig. 2. The total deformation rate is divided into viscoelastic and viscoplastic parts

$$\dot{\varepsilon}_{ij} = \dot{\varepsilon}_{ij}^{(e)} + \dot{\varepsilon}_{ij}^{(p)} \tag{24}$$

and the viscoelastic deformation rate has an elastic and a viscous component

$$\dot{\varepsilon}_{ij}^{(e)} = \dot{\varepsilon}_{ij}^{(k)(e)} + \dot{\varepsilon}_{ij}^{(k)(v)} \tag{25}$$

where $\dot{\varepsilon}_{ij}, \dot{\varepsilon}_{ij}^{(k)(e)}, \dot{\varepsilon}_{ij}^{(k)(v)}, \dot{\varepsilon}_{ij}^{(p)}$ are the total deformation rate, the k'th component elastic deformation rate, the k'th component viscous deformation rate, and the viscoplastic deformation rate, respectively.

The viscoelastic part is described by the set of equations

$$\frac{\dot{\sigma}_{ij}^{\prime(k)}}{2G_k} + \frac{\sigma_{ij}^{\prime(k)}}{\eta_k} = (\dot{\varepsilon}_{ij}^{\prime} - \dot{\varepsilon}_{ij}^{(p)}),\ k = 1, \ldots, n \tag{26}$$

for the stress deviators for the k'th Maxwell component, where G_k is the shear modulus and η_k is the viscosity for the k'th component. The primes indicate stress or deformation rate deviators. The total stress is the sum of the individual Maxwell component stresses

$$\sigma_{ij}^{\prime} = \sum_{k=1}^{n} \sigma_{ij}^{\prime(k)}. \tag{27}$$

For many polymers, the bulk response is non-linearly elastic with neglible viscosity. In this case, the trace of the total stress and deformation rates are related by

$$\dot{\sigma}_{ii} = 3K(\varepsilon_{ii})\dot{\varepsilon}_{ii} \tag{28}$$

where K is a volume and temperature dependent bulk modulus.

Finally, the total stress deviators are related to the viscoplastic deformation rate by the equation

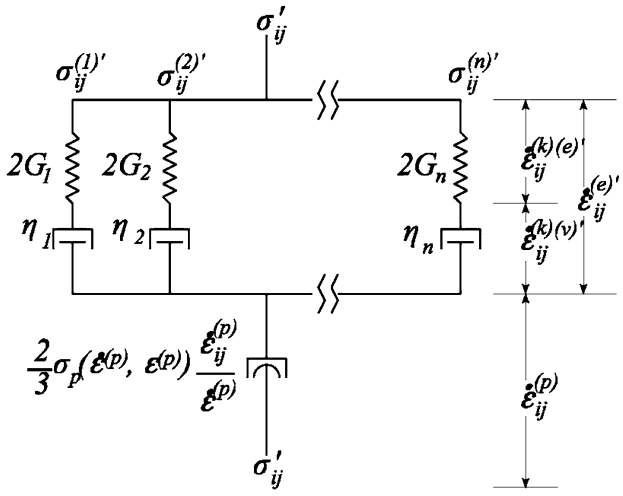

Fig. 2 Maxwell–Weichert linear viscoelasticity plus thermal activation non-linear viscoplasticity

$$\sigma_{ij}^{\prime} = \frac{2}{3}\sigma_p(\dot{\varepsilon}^{(p)}, \varepsilon^{(p)})\frac{\dot{\varepsilon}_{ij}^{(p)}}{\dot{\varepsilon}^{(p)}} \tag{29}$$

where $\sigma_p(\dot{\varepsilon}^{(p)}, \varepsilon^{(p)})$ is the function in Eq. 19 relating stress to strain rate and strain, and

$$\dot{\varepsilon}^{(p)} \equiv \sqrt{\frac{2}{3}\dot{\varepsilon}_{ij}^{(p)}\dot{\varepsilon}_{ij}^{(p)}} \tag{30}$$

is the effective deformation rate. While Eq. 29 looks deceptively like Mises plasticity, the diameter of the yield surface shrinks to zero as the plastic deformation rate goes to zero, so that it is possible to have a finite plastic deformation rate for arbitrarily small stresses.

The viscosities, or equivalently, the relaxation times, $\tau_k = \eta_k/2G_k$, have a temperature and pressure dependence given by

$$\tau_k = \tau_{0k}e^{H_k/T} \tag{31}$$

where the activation energies (in units of temperature) are

$$H_k = H_{0k} + A_{pk}p. \tag{32}$$

For the case of uniaxial stress, the equations reduce to the system of equations

$$\dot{\sigma}_{11}^{(k)} + \frac{\sigma_{11}^{(k)}}{\tau_k} = \frac{3G_kK}{K + \frac{1}{3}G_0}(\dot{\varepsilon}_{11} - \dot{\varepsilon}_{11}^{(p)}) + \frac{G_k}{3(K + \frac{1}{3}G_0)}\sum_{k'=1}^{n}\frac{\sigma_{11}^{(k')}}{\tau_{k'}},\quad k = 1, \ldots, n \tag{33}$$

and

$$\sigma_{11} = \sigma_p\left(\dot{\varepsilon}^{(p)}, \varepsilon^{(p)}\right)\frac{\dot{\varepsilon}_{11}^{(p)}}{|\dot{\varepsilon}_{11}^{(p)}|} \tag{34}$$

where G_0 is the unrelaxed modulus, $G_0 = \sum_{k=1}^{n} G_k$.

Application to polytetrafluoroethylene

Structure of PTFE

Despite the advantage of rather uniform plastic yielding behavior, PTFE has an unusually complicated phase diagram with four crystalline forms and a liquid phase [35]. The polymer chains are linear, composed of $-CF_2-$ groups, with the carbon atoms arranged in a zigzag pattern with a periodic 180° twist [36]. The chains pack in an approximately hexagonal arrangement. At

atmospheric pressure, below 293 K, the twist period comprises 13 CF_2 groups, and the crystal structure is triclinic [37] (Phase II) with unit cell parameters $a = 0.561$ nm and c (twist period along polymer chain) = 1.68 nm. At atmospheric pressure, at temperatures greater than 293 K (20 °C), the twist period increases to 15 CF_2 groups, and a partially disordered hexagonal crystal is formed (Phase IV) with unit cell parameters $a = 0.566$ nm and $c = 1.95$ nm. Above 303 K (30 °C) the crystal is pseudo-hexagonal with a random twist period (Phase I) and a crystalline melting point [38, 39] of 600 K. At pressures above about 450–700 MPa, the periodic twist disappears and the chains assume a planar zig-zag form [40] arranged in a monoclinic crystal structure (Phase III). Phases I, II, and III meet at a triple point at approximately 343 K (70 °C) and 450 MPa. The amorphous part of the material has several glass-like transition temperatures, designated α, β, and γ by McCrum [41, 42]. The γ transition is variously quoted as being somewhere in the range of 130–250 K. Lau et al. [43] review the published results and conclude that the transition is very broad, covering the range 160–240 K with the midpoint at about 200 K. The highest temperature amorphous transition, designated α, occurs at about 400 K and the β transition occurs at about 320 K.

Most of the experimental constitutive data for PTFE used for the analysis in this work lies in the temperature and pressure range in which the crystal is triclinic and the amorphous material is above the γ transition and below the β transition. It is not known, therefore, how accurately the constitutive equation will predict the mechanical behavior of PTFE in other regions of the phase diagram. There is also insufficient experimental data available to determine whether there is a significant pressure dependence in the thermal activation coefficients α and β described in Eq. 20 above.

Data analysis: viscoplastic component

The parameters for use in the constitutive equation were obtained by analyzing results reported by a number of investigators: compressive split Hopkinson pressure bar stress–strain curves at a number of strain-rates reported by Walley and Field [44], a low temperature (130 K) Hopkinson bar stress–strain curve reported by Walley et al. [45], Hopkinson bar data at a number of temperatures and strain-rates determined by Gray [46], and tensile stress–strain data at various superposed hydrostatic pressures reported by Sauer and Pae [47]. The parameters derived from these data are given in Table 1. A brief description of the analysis leading to these parameters is given in Appendix A.

Data analysis: linear viscoelastic component

An eight component Maxwell–Weichert model was used for the viscoelastic part, with the moduli, relaxation times, and activation energies, G_k, τ_{0k}, H_{0k}, respectively, chosen to give a reasonably good match to the shear storage modulus and logarithmic decrement versus temperature data at 1 Hz published by McCrum [48] as shown in Figs. 3 and 4. As discussed above, this type of model consideration is hoped to lead eventually to a physical model description of the internal relaxation mechanisms. The storage modulus in the Maxwell–Weichert model is given by the expression

$$G'(\omega, T) = \sum_{k=1}^{n} G_k \frac{[\omega\tau_k(T)]^2}{1 + [\omega\tau_k(T)]^2} \tag{35}$$

and the logarithmic decrement reported by McCrum is

$$\delta = \frac{1}{2}\frac{G''(\omega, T)}{G'(\omega, T)} \tag{36}$$

where

$$G''(\omega, T) = \sum_{k=1}^{n} G_k \frac{\omega\tau_k(T)}{1 + [\omega\tau_k(T)]^2} \tag{37}$$

is the loss modulus. With eight components, the match is good except at the highest temperatures near the melting point.

For the purpose of the comparisons presented here, it was assumed that PTFE can be treated as incompressible, so that Eq. 33 simplifies considerably, and the effective elastic (Young's) moduli, E_k, are three times the shear moduli, G_k. While some calculations were performed using a temperature dependent bulk modulus approximating that for PTFE, the results are not significantly different and the precision of the data does not warrant the slightly more accurate calculations.

Table 1 Parameters for the viscoplastic deformation of PTFE

β_0 (K^{-1})	2.01×10^{-2}
β_1 (K^{-1})	2.64×10^{-4}
α_0 (K^{-1})	4.78×10^{-3}
α_1 (K^{-1})	5.02×10^{-5}
ω_a	–3.6
ω_b	–0.625
ω_p (MPa^{-1})	–0.04
B_{pa} (MPa)	4016
B_{pb}	2.0×10^{-2}
B_{pn}	0.714
B_{0pa} (MPa)	72.4
B_{0pb}	2.2×10^{-2}
B_{0pn}	0.5

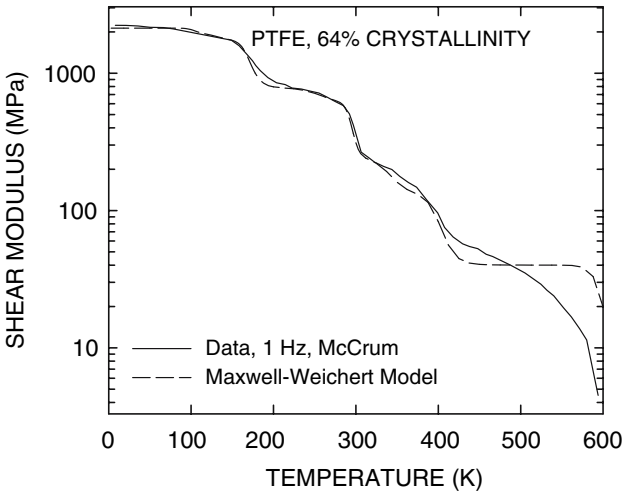

Fig. 3 Fit of Maxwell–Weichert model with eight components to storage shear modulus data of McCrum [48] for 64% crystallinity PTFE at 1 Hz. The data cover the temperature range from 4.2 K to the melting point at 600 K

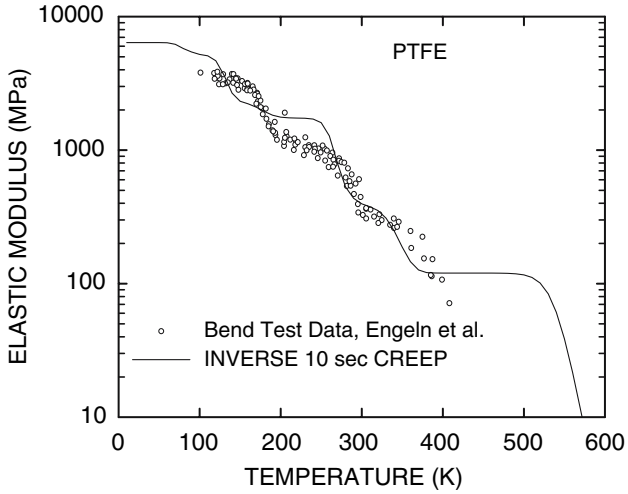

Fig. 5 10 s stress relaxation modulus calculated with eight component Maxwell–Weichert model compared to bend test data reported by Engeln et al. [49] on drawn specimens of 42% crystallinity PTFE

It is of interest to compare the elastic moduli calculated with this model with independently measured elastic moduli. Figure 5 shows the results calculated with the parameters in Table 2 compared with bend test data reported by Engeln et al. [49] on uniaxially drawn specimens of 42% crystallinity PTFE. From their description of the test, we conclude that they effectively measured the 10 s creep compliance. In Fig. 5, we have plotted the reciprocal of the calculated 10 s creep compliance to compare with the reported bend test moduli. The agreement is reasonable, considering that the test data refers to a variety of drawn specimens of lower crystallinity material than that for which the model parameters were derived. Note that the data clearly show the effect of the amorphous transition at 200 K and the amorphous and crystalline transitions at 300–320 K.

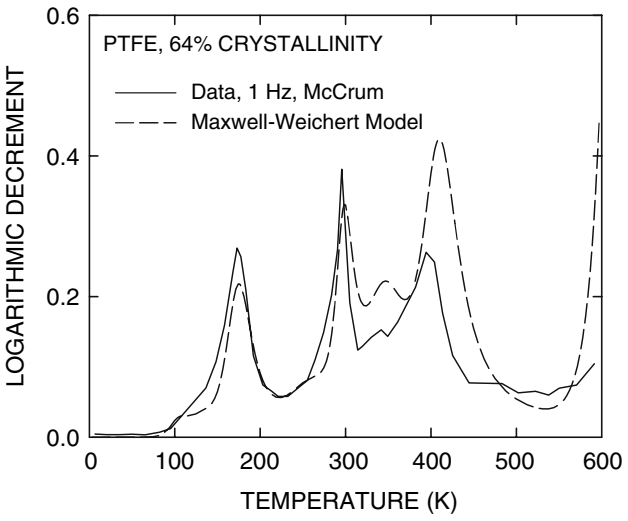

Fig. 4 Fit of Maxwell–Weichert model with eight components to logarithmic decrement data for 64% PTFE at 1 Hz. The data of McCrum [48] cover the temperature range from 4.2 K to the melting point at 600 K

The creep compliance may be calculated in a number of ways, all of which are time consuming. The direct method is integration of the differential equations under the constraint of constant total stress. Another method is to calculate the stress relaxation modulus for each temperature with the expression

$$E_R(t,T) = \sum_{k=1}^{n} E_k \exp[-t/\tau_k(T)]. \tag{38}$$

and convert it to a creep compliance curve with the numerical method of Hopkins and Hamming [50]. The best method is to find the equivalent Kelvin–Voigt model for each temperature that gives the parameters for the expression

Table 2 Maxwell–Weichert parameters for the initial linear viscoelastic deformation of PTFE

k	G_k (MPa)	τ_{0k} (s)	H_{0k} (K)
1	950	1.7×10^{-7}	2,338
2	350	2.2×10^{-17}	10,740
3	90	5.1×10^{-12}	9,640
4	100	4.6×10^{-9}	5,920
5	40	4.1×10^{-18}	22,920
6	200	2.7×10^{-5}	1,160
7	200	2.1×10^{-5}	2,320
8	200	4.2×10^{-6}	1,106

$$J(t,T) = J_0 + \sum_{k=1}^{n} J_k(T)[1 - \exp(-t/\tau_k(T))] + \frac{t}{\eta(T)} \tag{39}$$

from which the creep compliance may be calculated. After all is said and done, the calculations show that the reciprocal of the 10 s creep compliance does not differ significantly from the 10 s relaxation modulus, given by Eq. 38.

In another comparison, shown in Fig. 6, we have plotted the calculated stress relaxation modulus versus time at 293 K and compared it with test data published by Nagamatsu et al. [51]. They reduced their data to a master curve at 293 K and that is plotted in Fig. 6. Their master curve covers the range from one second to 10^{14} s and there is reasonable agreement between the calculation and the data in the range between 1 and 100 s. The calculation does not reproduce the test results for times greater than 100 s, but this is not of concern here, because we only intend to describe the high rate, short time behavior.

The viscoelastic pressure volume of activation A_p was assumed to have the same value for each Maxwell element. It was set at a value of 4.0 K/MPa so that the calculated initial slope of the stress–strain curve would match that of the data of Sauer and Pae at the highest pressure (552 MPa) at which they measured the stress–strain curve.

Complete constitutive equation for PTFE

With both the viscoplastic and viscoelastic components of the constitutive equation, we are now able to integrate the set of differential equations (31)–(34) to construct the complete stress–strain relation. Figures 7–10 show the complete stress–strain curves calculated with the parameters in Tables 1 and 2 compared to the reported experimental data.

In Fig. 7, the compressive Hopkinson bar data for stress vs. strain at six strain rates ranging from 0.016 s^{-1} to 22,600 s^{-1} reported by Walley and Field [44] are compared to the results calculated with Eqs. 31–34. The change in shape of the curves with strain rate is well reproduced. Results over a range in temperature and mostly at lower strain rates, that are of less interest, were obtained by Rae et al. [52], and including pressure-induced phase transformation at higher temperatures and higher imposed strain rates [53, 54], appear to be in line with the expectation from those results shown here only at the higher strain rates.

In Fig. 8, compressive Hopkinson bar data (at high strain rate) for stress versus strain at seven temperatures, as reported by Gray [55] are compared to the results calculated with Eqs. 31–34. The calculated stresses agree well with the observed stresses.

In Fig. 9, the compressive Hopkinson bar data for stress vs. strain two temperatures, 130 K and 300 K, reported by Walley et al. [45] are compared to the

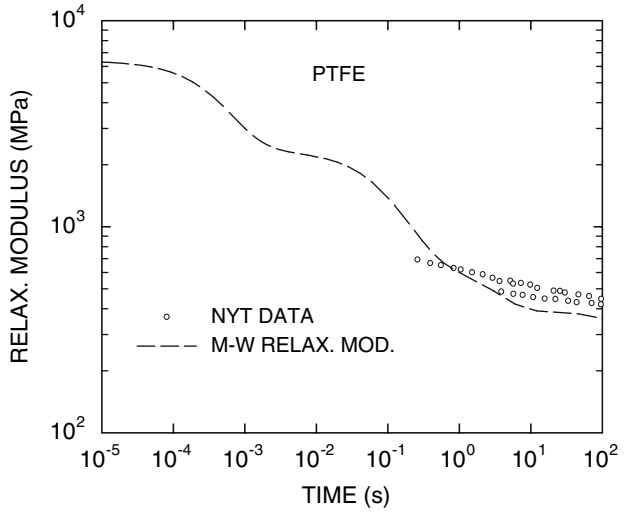

Fig. 6 Stress relaxation modulus at 293 K vs. time, calculated with eight component Maxwell–Weichert model, compared to master curve reported by Nagamatsu et al. [51]

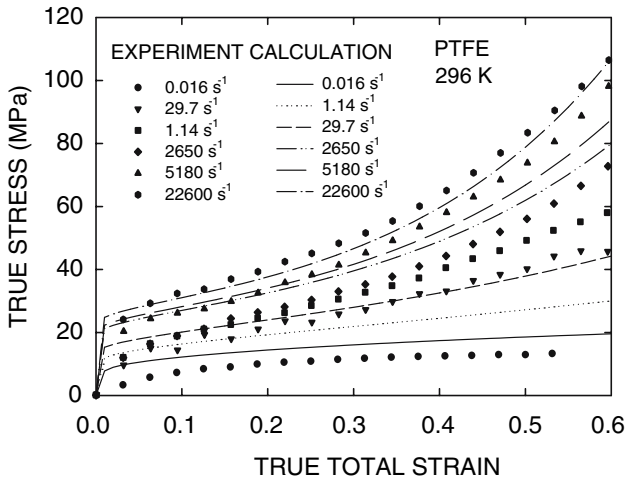

Fig. 7 Total stress–strain calculated with Eqs. 19 and 31–34 and the parameters in Tables 1 and 2, compared with split Hopkinson pressure bar data reported by Walley and Field [44] for PTFE

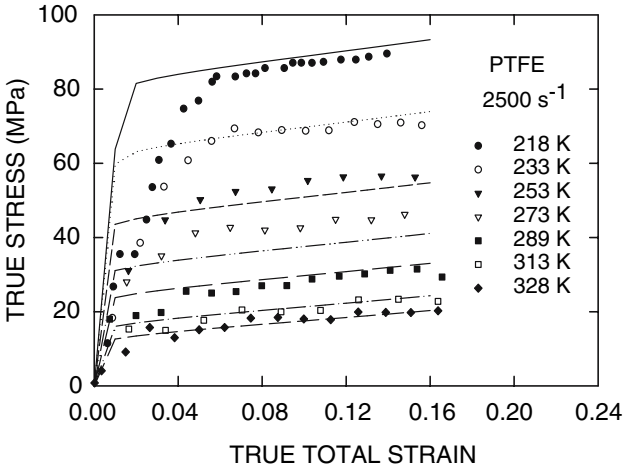

Fig. 8 Total stress–strain calculated with Eqs. (19) and (31–34) and the parameters in Tables 1 and 2, compared with split Hopkinson pressure bar data reported by Gray [55] for PTFE

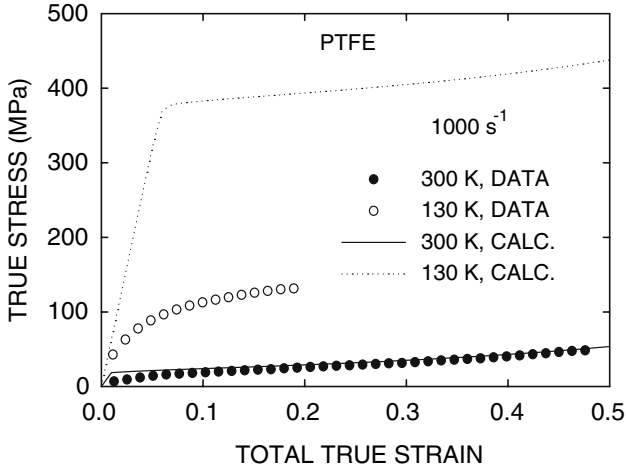

Fig. 9 Total stress–strain at 130 K calculated with Eqs. (19) and (31–34) and the parameters in Tables 1 and 2, compared with split Hopkinson pressure bar data reported by Walley, Field, Pope, and Safford [45] for PTFE

results calculated with Eqs. 31–34. At 130 K, the calculated stress is much higher than the observed stress. Because 130 K is far below the γ transition temperature, the material is very likely to be brittle, so that the observed strength may have been compromised by fracture of the material.

In Fig. 10, tensile stress–strain with superimposed hydrostatic pressure data reported by Sauer and Pae [47] are compared to results calculated with Eqs. 31–34. The change of shape of the curves with pressure is well reproduced.

Application to polymethylmethacrylate

The yield stress of polymethylmethacrylate

As discussed with respect to Fig. 1, the thermal activation model was applied to yield stress data obtained by Bauwens-Crowet [3] for polymethylmethacrylate (PMMA) at various temperatures and strain rates; and, it was shown that a volume of activation inversely proportional to the yield stress gave good agreement between the calculated and measured yield stresses. The key to obtaining good agreement between the model and the experimental data is to account for the dependence of the non-linear viscoplastic flow mechanisms on the small strain shear modulus which has a strong variation with temperature [56].

In Fig. 11, Bauwens-Crowet's data for the compressive yield stress of PMMA divided by its shear modulus is plotted as a function of the quantity $T\ln(\dot{\varepsilon}_0/\dot{\varepsilon}) = G/k$. With the correct choice of $\dot{\varepsilon}_0$, the equality holds, the quantity is the activation energy in degrees Kelvin, and the data in the plot should coalesce into a single one-parameter curve, as it does in the figure with the choice of $\dot{\varepsilon}_0 = 2 \times 10^7$ s^{-1}.

Furthermore, with the volume of activation being inversely proportional to the effective shear stress, then a curve in an ln (stress) plot should be a straight line with slope $-k/W_0$ and intercept $ln\ (B/\mu)$. An inspection of Fig. 11 shows this to be very closely the case, with $k/W_0 = 2.56 \times 10^{-4}$ K^{-1} and $B/\mu =$ 0.454. These parameters then give calculated values of yield stress versus strain rate and temperature which match well with Bauwens-Crowet's data. Recently, Fleck et al. [15] have employed the Bauwens-Crowet yield results described with a "two-element Eyring equation" to relate to the onset of PMMA fracturing behavior.

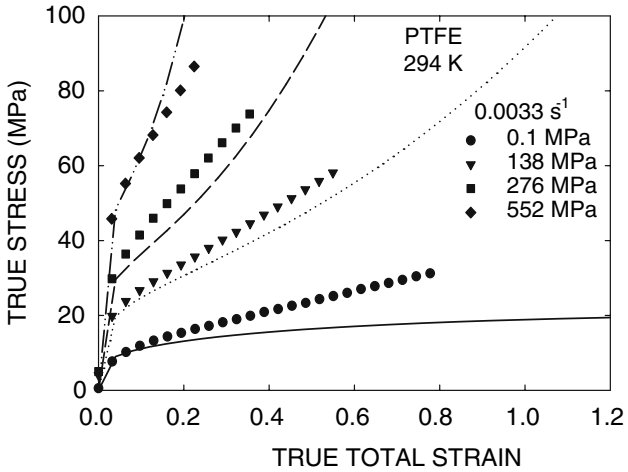

Fig. 10 Total stress–strain calculated with Eqs. (19) and (31–34) and the parameters in Tables 1 and 2, for different pressures, compared with tensile test data reported by Sauer and Pae [47]

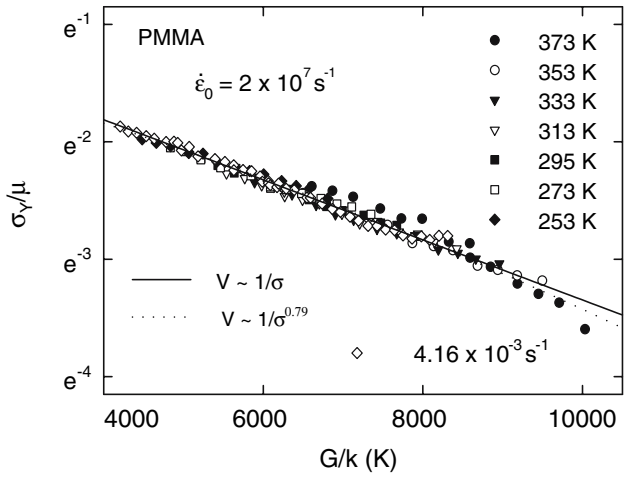

Fig. 11 Compressive yield stress divided by shear modulus versus G/k for PMMA. Data of Bauwens-Crowet [3] is shown by the symbols. The solid line is the model fit for a volume of activation inversely proportional to effective shear stress, while the dotted curve is the result of a fit for a more general inverse power dependence

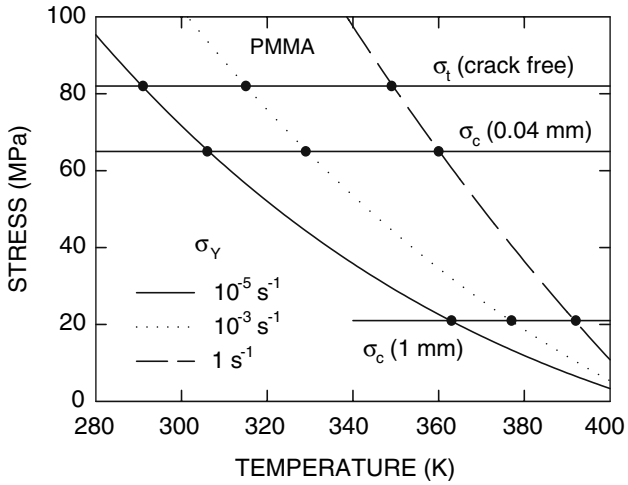

Fig. 12 Ductile-brittle transition temperature in PMMA for strain rates from 10^{-5} s^{-1} to 1 s^{-1} and crack sizes from 1 mm to zero (crack free material). The material is brittle for temperatures below the point of intersection of the yield stress curve, for a given strain rate, with the fracture stress, for a given crack size

The PMMA ductile–brittle transition

The yield stress results obtained in compression for PMMA at different temperatures and strain rates may be compared with predictions of a transition to brittle fracturing when tested in tension. The pre-cracked brittle fracture stress of PMMA, σ_c, is known to follow the relation [57]

$$\sigma_c = \sigma_t[s/(c+s)]^{1/2}, \tag{40}$$

where σ_t is the crack-free tensile fracture stress and s is the width of a zone of plastic yielding at the tip of a crack of radius c. This relation is a very good approximation to the more rigorous result of Bilby et al. [58]. From an analysis of the fracture stress data for PMMA reported by Berry [59], σ_t is determined to be 82 MPa and s is 0.068 mm.

A tensile ductile–brittle transition may be defined for PMMA and related polymers by the condition

$$\sigma_y(T,\dot{\varepsilon}) = \sigma_c(T,\dot{\varepsilon}), \tag{41}$$

where at larger crack sizes σ_c is normally taken on a fracture surface energy basis to be relatively independent of temperature and strain rate. At smaller crack sizes, a more significant temperature and strain rate dependence may enter for σ_c. Equation 41 provides a means of calculating the ductile–brittle transition temperature as a function of strain rate, as illustrated in Fig. 12. Thus, for example, for an intentional crack radius of 1.0 mm, and strain rate of 0.001 s^{-1}, brittle tensile fracture should occur before yield at all temperatures less than 377 K, whereas for a smaller unintentional crack radius of 0.04 mm, and strain rate of 1.0 s^{-1}, brittle fracture would occur at yield for T ~360 K, and before yield at temperatures less than 360 K.

Conclusion

A constitutive equation has been developed that describes reasonably well both the effective stress for viscoplastic flow in PTFE in uniaxial dynamic tension tests as a function of strain, strain rate, temperature, and the pressure and the yield stress of PMMA as a function of temperature and strain rate. A key element of the analysis is employment of an inverse stress dependence of the (shear) activation volume for thermally activated flow units. The upward curvature of the strain hardening curve for polymers is accounted for by a pressure and strain rate dependent rate of immobilization of flow units. The model does not describe long term relaxation or creep effects. It should, due to the inclusion of pressure dependence, predict the difference in stress between compressive and tensile loading. For polymers that display a strain-softening after a yield point, the yield term in the viscoplastic stress equation (19) may be given a strain dependence using the same analysis that was applied to the strain hardening term.

Acknowledgements This work was principally supported by the NSWC Independent Research Program with partial support from the Office of Naval Research. Additional partial support

was provided by NSWC for Ronald Armstrong. Appreciation is expressed to Stephen Mitchell and Wayne Reed for the NSWC IR support, Chester Clark for the NSWC support, and to Judah Goldwasser for the ONR support. Appreciation is also expressed to G. T. Gray, III for providing us his Hopkinson bar data on PTFE in advance of publication.

Appendix A: Obtaining parameters for the viscoplastic element

Each stress–strain curve not already reported as true stress-true strain is transformed to true stress-true strain with the formulae

$$\begin{aligned} \sigma &= S(1+e) \\ \varepsilon &= \ln(1+e) \end{aligned} \tag{A1}$$

where S and e are load and elongation, respectively, and σ and ε are true stress and true strain, respectively. While this transformation applies only if the flow is volume conserving, the error in applying it to the entire stress–strain curve is generally small. Then, for each curve, a guess is made for the initial linear viscoelastic modulus, and the elastic strain is subtracted from the total strain to obtain the viscoplastic strain. Each true stress–viscoplastic strain curve is then fitted to an equation of the form

$$\sigma = \sigma_0 + K\sqrt{(1-e^{-\omega\varepsilon})/\omega} \tag{A2}$$

and σ_0 is obtained from the intercept (or extrapolated intercept) with the σ-axis at zero viscoplastic strain. K and ω could be obtained with a non-linear least squares fit to the data, but a quicker and better result is obtained simply by solving for K and ω by taking two points on the curve, one near the end, at large strain, and one at half that strain.

To obtain B, β_0, and β_1, write

$$\ln\sigma_0 = \ln B - \beta_1 T \ln(\dot{\varepsilon}_{0\beta}/\dot{\varepsilon}) \tag{A3}$$

where $\beta_0 = \beta_1 \ln\dot{\varepsilon}_{0\beta}$. Pick an $\dot{\varepsilon}_{0\beta}$, and plot $\ln\sigma_0$ against $T\ln(\dot{\varepsilon}_{0\beta}/\dot{\varepsilon})$. With the best value of $\dot{\varepsilon}_{0\beta}$, all the data points will lie on or close to a single straight line whose slope is $-\beta_1$ and intercept is $ln\ B$. Similarly, to obtain B_0, α_0, and α_1, write

$$\ln K = \ln B_0 - \alpha_1 T \ln(\dot{\varepsilon}_{0\alpha}/\dot{\varepsilon}). \tag{A4}$$

Finally, the dependence of ω on strain rate and pressure may be determined by a linear regression and the pressure dependence of B and B_0 may be determined by a series of linear regressions with differing trial exponents.

References

1. Eyring H (1935) J Chem Phys 3:107
2. Eyring H (1936) J Chem Phys 4:283
3. Bauwens-Crowet C (1973) J Mater Sci 8:968
4. Fotheringham D, Cherry BW (1976) J Mater Sci 11:1368
5. Bauwens-Crowet C (1976) J Mater Sci 11:1370
6. Armstrong RW (1973) (Indian) J Sci Indust Res 32:591
7. Zerilli FJ, Armstrong RW (1992) Acta Metall Mater 40:1803
8. Li JCM (1982) In: Escaig B, G'Sell C (eds) Plastic deformation of amorphous and semicrystalline materials. Publ les Ulis, Les editions de physique, France, p 29
9. Rivier N, Gilchrist H (1985) J Non-Cryst Sol 75:259
10. Rivier N (1994) Sol State Phenom 35:107
11. Porter D (1995) Group interaction modeling of polymer properties. Marcel Dekker, New York
12. Porter D (1997) J Non-Newtonian Fluid Mech 68:141
13. Walley SM, Field JE (1994) DYMAT J 1:211
14. Briscoe BJ, Nosker RW (1985) Polymer Comm 26:307
15. Fleck NA, Stronge WJ, Liu JH (1990) Proc Roy Soc Lond A429:459
16. Tschoegl NW (1989) The phenomenological theory of linear viscoelastic behavior. Springer-Verlag, Berlin, p 158
17. Zener C (1948) Elasticity and anelasticity of metals. University of Chicago Press, Illinois, p 43
18. Johnston WG, Gilman JJ (1959) J Appl Phys 30:129
19. Krausz AS, Eyring H (1975) Deformation kinetics. Wiley, New York
20. Perzyna P (1966) Advances in applied mechanics, vol 9. Academic Press, New York
21. Bardenhagen SG, Stout MG, Gray GT III (1997) Mech Mater 25:235
22. Thomas DA (1969) Polymer Eng Sci 9:415
23. Sauer JA, Mears DR, Pae KD (1970) Euro Polymer J 6:1015
24. Christiansen AW, Baer E, Radcliffe SV (1971) Philos Mag 24:451
25. Joseph SH, Duckett RA (1978) Polymer 19:837
26. Davis LA, Pampillo CA (1971) J Appl Phys 42:4659
27. Pae KD (1977) J Mater Sci 12:1209
28. Hu LW, Pae KD (1963) J Franklin Inst 275:491
29. Escaig B (1978) Ann Phys France 3:207
30. Hasan OA, Boyce MC (1993) Polymer 34:5085
31. Kauzmann W (1941) Trans Am Inst Min Metall Eng 143:57
32. Gilman JJ (1973) J Appl Phys 44:675
33. Bergstrom Y (1970) Mater Sci Eng 5:193
34. Argon AS (1973) Philos Mag 28:839
35. Flack HD (1972) J Polymer Sci A-2 10:1799
36. Sperati CA, Starkweather HW Jr (1961) Fortschr Hochpolym-Forsch (Adv Polymer Sci) 2:465
37. Weeks JJ, Clark ES, Eby RK (1981) Polymer 22:1480
38. Pistorius CWFT (1964) Polymer 5:315
39. Rigby HA, Bunn CW (1949) Nature 164:583
40. Bunn CW, Howells ER (1954) Nature 174:549
41. McCrum NG (1959) Makromol Chem 34:50
42. McCrum NG, Read BE, Williams G (1967) Anelastic and dielelectric effects in polymeric solids. Wiley, New York
43. Lau S, Wesson JP, Wunderlich B (1984) Macromolecules 17:1102
44. Walley SM, Field JE (1994) DYMAT J 1:211, Fig. 20
45. Walley SM, Field JE, Pope PH, Safford NA (1991) J Phys III France 1:1889, Fig. 161
46. Gray GT III (1998) In: Khan AS (ed) Proceedings of plasticity '99, the seventh intern. symp. on plasticity and its current applications. Neat Press, Fulton, MD
47. Sauer JA, Pae KD (1974) Colloid Polymer Sci 252:680

48. McCrum NG (1959) J Polymer Sci 34:355
49. Engeln I, Hengl R, Hinrichsen G (1984) Colloid Polymer Sci 262:780
50. Hopkins IL, Hamming RW (1957) J Appl Phys 28:906
51. Nagamatsu K, Yoshitomi T, Takemoto T (1958) J Colloid Sci 13:257
52. Rae PJ, Dattelbaum DM (2004) Polymer 45:7615
53. Rae PJ, Brown EN, Clements BE, Dattelbaum DM (2005) J Appl Phys 98:063521
54. Rae PJ, Gray GT III, Dattelbaum DM, Bourne NK (2005) In: Furnish MD, Gupta YM, Forbes JW (eds) Shock compression of condensed matter – 2004. Amer Inst Phys, Melville NY, p 671
55. Gray GT III (1997) Methods in materials research. Wiley, New York
56. Zerilli FJ, Armstrong RW (2000) In: Furnish MD, Chhabildas LC, Hixon RS (eds) Shock compression of condensed matter – 1999. AIP Conf. Proc. CP505, Am Inst Phys, Melville, New York, p 531
57. Armstrong RW (1973) In: Kochendorfer A (ed) Third international conference on fracture. Verein Deutscher Eisenhuttenleute, Munich, Paper III-421
58. Bilby BA, Cottrell AH, Swinden KH (1963) Proc Roy Soc Lond A272:304
59. Berry JP (1964) In: Rosen B (ed) Fracture processes in polymeric solids. Interscience Wiley, New York, p 195